

J1615+5452: a remnant radio galaxy in the ELAIS-N1 field

Z. Randriamanakoto^{1*}, C. H. Ishwara-Chandra², A. R. Taylor^{3,4}

¹South African Astronomical Observatory, P.O. Box 9, Observatory 7935, South Africa

²National Centre for Radio Astrophysics, TIFR, Post Bag No. 3, Ganeshkhind Post, 411007 Pune, India

³Inter-University Institute for Data Intensive Astronomy, and Department of Astronomy, University of Cape Town, Private Bag X3, Rondebosch 7701, South Africa

⁴Inter-University Institute for Data Intensive Astronomy, and Department of Physics and Astronomy, University of the Western Cape, Private Bag X17, Bellville 7535, South Africa

Accepted 2020 June 16. Received 2020 June 16; in original form 2019 November 30

ABSTRACT

We report the discovery of a remnant radio AGN J1615+5452 in the field of ELAIS-N1. GMRT continuum observations at 150, 325 and 610 MHz combined with archival data from the 1.4 GHz NVSS survey were used to derive the radio spectrum of the source. At a redshift $z \sim 0.33$, J1615+5452 has a linear size of ~ 100 kpc and spectral indices ranging between $\alpha_{610}^{1400} < -1.5$ and $\alpha_{150}^{325} = -0.61 \pm 0.12$. While the source has a diffuse radio emission at low frequencies, we do not find evidence of core, jets or hotspots in the 1.4 GHz VLA data of ~ 5 arcsec angular resolution. Such morphological properties coupled with a curved radio spectrum suggest that the AGN fueling mechanisms undergo a shortage of energy supply which is typical of a dying radio AGN. This is consistent with the observed steep curvature in the spectrum $\Delta\alpha \approx -1$, the estimated synchrotron age of $t_s = 76.0_{-8.7}^{+7.4}$ Myr and a t_{off}/t_s ratio of ~ 0.3 .

Key words: galaxies: active – galaxies: individual: J1615+5452 – radio continuum: galaxies.

1 INTRODUCTION

In the active stage which usually lasts ~ 10 – 100 Myr (Cordey 1986), the classical morphology of a radio galaxy is characterized by the presence of a core, a pair of lobes and including jets, and/or hotspots. Such features indicate the continuous injection (CI) of relativistic electrons that fuel the active galactic nuclei (AGN). Following the active phase of the radio AGN, the source enters the so-called remnant or dying phase, as the nuclear engine switches off and the compact radio components, typical signatures of current activity, eventually disappear (Parma et al. 1999; Slee et al. 2001; Kapińska et al. 2010; Morganti 2017).

Despite the challenges of detecting radio AGNs in their remnant phase, especially prior to the era of low frequency radio facilities such as the Giant Metrewave Radio Telescope (GMRT, Swarup 1991), the Low-Frequency ARray (LOFAR, van Haarlem et al. 2013) and the Murchison Widefield Array (MWA, Lonsdale et al. 2009; Tingay et al. 2013), Cordey (1987) made a breakthrough when reporting the first discovery of a dying AGN known as B2 0924+30. Since then, this prototype of genuine radio remnants hosted by IC 2476 has been the subject of follow-up studies (Jamrozy et al. 2004; Shulevski et al. 2017; Turner 2018). Meanwhile, other

sources of this type have now been found in wide-field radio surveys (e.g. Parma et al. 2007; Murgia et al. 2011; Saripalli et al. 2012; de Gasperin et al. 2014; Brienza et al. 2016, 2017; Mahatma et al. 2018; Duchesne & Johnston-Hollitt 2019).

The switching off of the central AGN activity is translated into a steep spectrum $\alpha < -1.3$ ($S \propto \nu^\alpha$, e.g. Komissarov & Gubanov 1994; Parma et al. 2007; Shulevski et al. 2017) of the associated radio emission in the GHz frequency regime, according to radiative ageing models (e.g. Kardashev 1962; Pacholczyk 1970; Jaffe & Perola 1973). This is because the injected relativistic electrons lose energy with time due to both synchrotron emission and Inverse Compton scattering with the Cosmic Microwave Background (CMB) photons (Komissarov & Gubanov 1994). Since higher energy electrons lose energy more quickly and have shorter radiative lifetimes, this results in a high-frequency turn down of the synchrotron spectrum occurring beyond a break frequency ν_b that drifts in time to lower frequencies. Below the break frequency, the radio spectrum of the non-active source has a spectral injection index, α_{inj} , typically in the range < -0.5 to -1 (e.g. Blandford & Ostriker 1978; Murgia et al. 2011; Brienza et al. 2016), while above ν_b , the spectral index α is steeper than $\alpha_{\text{inj}} - 0.5$ (Kardashev 1962; Pacholczyk 1970; Jaffe & Perola 1973).

Searches for remnant radio AGNs are generally based on detection of ultra-steep spectra at low frequencies (e.g.

* E-mail: zara@sao.ac.za

Parma et al. 2007; Cohen et al. 2007). To recover candidates with a spectrum not steep enough at low frequencies but ultra-steep above ~ 1.4 GHz, Murgia et al. (2011) and Brienza et al. (2016, 2017), following the idea of Sohn et al. (2003), used the radio spectral curvature parameter (SCP). This parameter uses multi-frequency information to examine the difference between high frequency and low frequency spectral indices, i.e. $\Delta\alpha = \alpha_{\text{high}} - \alpha_{\text{low}}$, and its value correlates with the different evolutionary stages of the radio galaxy. In the typical case of a remnant AGN, $\Delta\alpha \ll -0.5$ (Murgia et al. 2011).

Since remnant AGNs represent the final stage in the evolution of a radio galaxy, they are important objects for understanding of the radio galaxy life cycle, i.e. from the triggering of relativistic jets to the nuclear engine switch off, possibly followed by a restarting activity of AGN that may co-exist with a surrounding fossil radio emission (Saikia & Jamrozy 2009; Murgia et al. 2011; Saripalli et al. 2012; Shulevski et al. 2012; Konar et al. 2013; Morganti 2017; Mahatma et al. 2018; Jurlin et al. 2020). Characterizing these elusive objects through their morphology and spectra will help determine the duty cycle of the radio core activity and the dynamical evolution of radio galaxies since mechanisms such as adiabatic expansion and radiative losses are expected to regulate the evolution of the remnant radio plasma once the radio jets switch off. Thorough investigations of the AGN duty cycle and its dynamics are thus crucial to put constraints on the radio galaxy evolution models (e.g. Brienza et al. 2017; Mahatma et al. 2018; Shabala et al. 2020). An extensive analysis of these sources will also help to address one of the key questions in the field of galaxy evolution: the co-evolution process between the supermassive black hole (SMBH) and its host galaxy (e.g. Silk & Rees 1998; Kormendy & Ho 2013; Sijacki et al. 2015). Although the tight correlation between the SMBH growth and the galaxy build-up has already been widely acknowledged, the impacts of the AGN physical properties and AGN feedback on the cosmic evolution of the host galaxy and its environment are still under debate (Jahnke & Macciò 2011; Fabian 2012 and references therein).

Because of the rapid timescale of particle energy decay, and the paucity of high sensitivity data at multiple wavelengths, only a handful of steep spectrum dying radio sources have been observed, especially in the cm wavelength regime. However, in addition to their spectral signature, fossil AGNs may be recognizable in deep low-frequency images as relatively bright and diffuse emission devoid of a core and/or hotspots and with resolutions of a few arcseconds. Such emission arises from low energy particles that are relatively unaffected by the fast spectral evolution (Parma et al. 2007; Murgia et al. 2011; Brienza et al. 2017; Morganti 2017).

In this work, we report the discovery of a new remnant radio galaxy, J1615+5452, in the field of the European Large-Area ISO Survey-North 1 (ELAIS-N1 or EN1, Oliver et al. 2000) from the GMRT 610 MHz observations. We use the archival low-frequency GMRT observations at 150 MHz and 325 MHz and 1400 MHz data from the Karl G. Jansky Very Large Array (VLA) to obtain the source radio spectrum and to reconstruct its history of AGN activity.

The paper is structured as follows. We describe the observations and data processing in Section 2. Radio morphology and integrated spectra of the source are reported in

Section 3 and Section 4 investigates the nature of the remnant AGN. We discuss the results in Section 5 and provide a summary of the work in Section 6. We adopt the following cosmological parameters throughout the paper: $H_0 = 67.8 \text{ km s}^{-1} \text{ Mpc}^{-1}$, $\Omega_{\text{m}} = 0.308$, and $\Omega_{\Lambda} = 1 - \Omega_{\text{m}}$ (Planck Collaboration et al. 2016).

2 OBSERVATIONS AND DATA PROCESSING

EN1 is a field in the northern part of the sky centred near RA = $16^{\text{h}}10^{\text{m}}$, DEC = $+54^{\circ}35'$ (J2000 coordinates). The low foreground infrared emission in this region has made it a primary target for deep extragalactic surveys, including deep radio continuum surveys over a range of frequencies (Garn et al. 2008; Sirothia et al. 2009; Grant et al. 2010; Banfield et al. 2011; Jelić et al. 2014; Taylor & Jagannathan 2016; Chakraborty et al. 2019; Ocran et al. 2020). This work uses observations of EN1 with the GMRT taken at 150, 325, and 610 MHz as well as data at 1400 MHz from the VLA. Table 1 summarizes the GMRT observation logs of the field including the central frequency, the bandwidth, the observing date and the on-source integration time.

2.1 GMRT observations

The 610 MHz data is from the ELAIS-N1 wide area survey of this region using the GMRT. This is a large area survey of 12.8 sq. degrees comprised of 51 pointings of 3 hours each and observed between 2011 and 2017 (Ishwara-Chandra et al. 2020, submitted). We used the GMRT Software Backend (GSB) with a 32 MHz bandwidth split into 256 spectral channels to avoid bandwidth smearing. On most days, we observed 3C286 as a primary calibrator while 3C48 for flux and bandpass calibration observed over a few days only. The data analysis was carried out using a fully automated CASA-based pipeline which is described in detail in Ishwara-Chandra et al. (2020, submitted). In a nutshell, the data was flagged, gain calibrated, and after which several rounds of self-calibration on target along with flagging on residuals were being processed. For imaging, we used a robust parameter of 0 in the Briggs weighting scheme. The final rms noise was $\sim 40 \mu\text{Jy}/\text{beam}$ at a resolution of 6 arcsec circular beam. J1615+5452 was discovered from this deep image as fuzzy source without any hotspots or compact feature. The angular extent of this source is much smaller than the largest source that can be detected at this frequency ($17''$).

The GMRT 325 MHz observations cover 3.6 square degree area of the ELAIS-N1 field with a phasecenter set at $\alpha = 16^{\text{h}}10^{\text{m}}$, $\delta = +54^{\circ}40'$. The survey is part of the GMRT radio continuum imaging of the Herschel/HerMES field (PI: Wadadekar, Prop ID: 24_026). Two single pointing observations of ≈ 8.5 hours each were carried on 2013 May 26 & 27 with a total bandwidth of ~ 32 MHz. Each ~ 52 min scan of the target field was followed by a ~ 5 min secondary calibrator observation to track the ionospheric conditions, the RFI contamination and any variations in the receiver system throughout the entire observing run. We have processed this archival data through the same CASA-based pipeline used to analyse the wide-area 610 MHz data. 3C286 and 3C48 were used for flux calibration and 1459+716 for phase calibration. Each day's data was calibrated separately and the

Table 1. Log of the GMRT observations of the ELAIS-N1 field.

Band [MHz]	Central Freqy [MHz]	BW [MHz]	Project Code & PI	Obs.date	On-source time [hr]	Resolution [arcsec]	σ_{rms} [$\mu\text{Jy}/\text{beam}$]
(1)	(2)	(3)	(4)	(5)	(6)	(7)	(8)
150	153	6	12MDB01, Dennefeld	May 2007	17 x 0.5	38 x 21	3500
325	323	32	24_026, Wadadekar	May 2013	2 x 8.5	9	70
610	610	32	19_064, 20_020, 21_086, 22_057, Taylor	2011 - 2017	3 x 1	6	40

Notes. Columns 1 & 2: nominal and precise central frequencies; Column 3: bandwidth used for mapping the field; Column 4: GMRT project code and name of the principal investigator; Column 5: date of the observations; Column 6: on-source integration time; Columns 7 & 8: angular resolution and rms noise of the radio image.

split files of target field were combined before imaging with CASA `tclean` using the default robust weighting of 0. We performed four rounds of phase-only self-calibration followed by five rounds of amplitude and self-calibration, which included residual-based flagging in between each round. The final image reached a sensitivity down to $\sigma \approx 70 \mu\text{Jy}/\text{beam}$ without applying direction-dependent calibration. Primary beam correction was done following standard procedures. J1615+5452 is clearly detected in this image and the source is much smaller than the largest angular size that can be imaged using the GMRT at 325 MHz ($\sim 30'$).

We searched for J1615+5452 in the 150 MHz TIFR GMRT Sky Survey (TGSS, Intema et al. 2017) and the source was not clearly detected. The nearest survey pointing center is 1.6 degree away which is close to the half-power beamwidth at 150 MHz. There is a faint source at the expected location with a peak flux density of about 20 mJy and a total flux density of $95 \pm 21 \text{ mJy}$. Since the peak flux is less than 5 times the local rms, it did not get listed in the TGSS catalogue. We searched for other 150 MHz archival data with the GMRT and found long observations with ~ 8.5 hours on-source time, taken in May 2007 (PI: Dennefeld). The signal bandwidth was 6 MHz with a correlator bandwidth of 8 MHz split into 128 channels to minimise the effects of bandwidth smearing. 3C147 and 3C48 were observed for primary calibration and 1459+716 for secondary calibration. The data was analysed using the SPAM pipeline (Intema et al. 2009) following standard procedure which included direction dependent calibration for total intensity continuum imaging (robust = 0). The rms noise of the image is $\sim 3.5 \text{ mJy}/\text{beam}$ with a resolution of 37.7×20.9 arcseconds at the position angle of 52 deg. The source is clearly detected in this image which is the one we use for the flux density estimate at 150 MHz (Table 2).

2.2 VLA observations at 1.4 GHz

A snapshot image of J1615+5452 is retrieved from the NRAO VLA Sky Survey (NVSS, Condon et al. 1998). At a resolution of ~ 45 arcsec coupled with a sensitivity of $\sim 2.5 \text{ mJy}/\text{beam}$ above 5σ , the 1.4 GHz survey records a flux density of 5.6 mJy for this given source. We also retrieved the radio image from the Faint Images of the Radio Sky at Twenty-Centimeters survey (FIRST, Becker et al. 1995), but the NVSS point-like source is only detected in FIRST below 4σ with a very weak intensity $< 0.4 \text{ mJy}$. We did not find radio counterparts as well in the 10 sq. degrees 1.4 GHz VLA image of the EN1 field published by Banfield et al. (2011). The local rms noise is $\sim 90 \mu\text{Jy}/\text{beam}$. Unlike NVSS, these two VLA observations are at a higher angular resolution of

~ 5 arcsec. No compact feature at high resolution suggests the absence of core emission.

3 PROPERTIES OF J1615+5452

3.1 Host galaxy

Figure 1 shows the 610 MHz radio continuum contours of J1615+5452 overlaid on a *i*-band image from the Sloan Digital Sky Survey Data Release 12 (SDSS-DR12, Alam et al. 2015). A red spheroidal galaxy is located coincident with the peak of the radio emission and slightly ~ 1.9 arcsec East of the centroid of the radio source. Based on spectroscopic observations from the SDSS-DR14 (Abolfathi et al. 2018), this galaxy has a redshift of $z = 0.32936 \pm 0.00005$ at which 1 arcsec corresponds to 4.89 kpc. With no obvious nebular emission lines from young blue stars, its integrated spectrum retrieved from the SDSS Catalog Archive Server¹ is rather characterized by a prominent break around 4000 Å and the presence of Ca H and K lines along with other strong absorption lines like MgI and NaD. Such features are typical of an early-type elliptical galaxy (Kennicutt 1992).

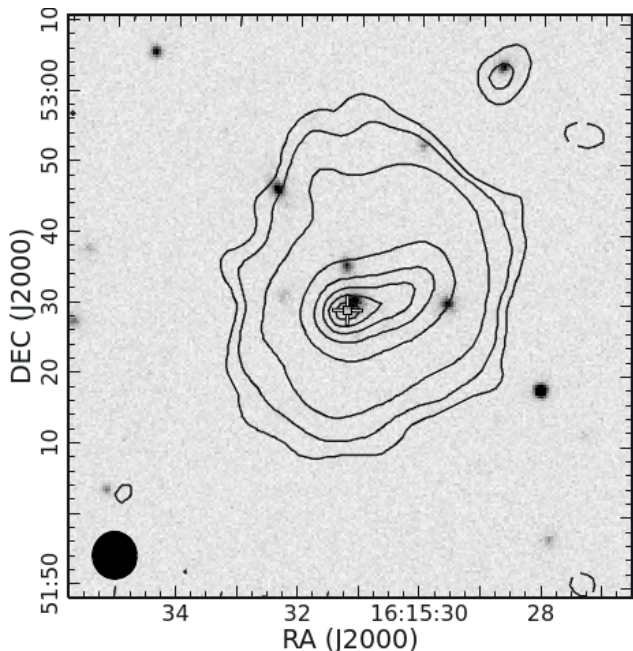
The newly detected remnant radio emission is likely associated with the SDSS galaxy. In fact, the slight misalignment between the position of the optical galaxy and the peak of the radio emission is consistent with a host galaxy that is moving away from the relic radio plasma after its AGN activity ceases (e.g. Duchesne & Johnston-Hollitt 2019). Such an offset has also been reported by Gentile et al. (2007) when studying 3C338, a restarted radio galaxy where the remnant plasma of the source is clearly disconnected from the host galaxy.

The potential host galaxy does not belong to any cluster of galaxies detected in EN1 field (V. Parekh, private communication). However, there are three SDSS galaxies with $g < 22$ mag within its $0.5'$ radius. Such a proximity to other galaxies suggests that the host galaxy could reside in a loose group environment. It is worth investigating the nature of the galaxy environment since Murgia et al. (2011) reported that fossil lobes of cluster-based remnant radio galaxies tend to be more confined than the ones associated with a dying radio source found in the field. Unfortunately, no X-ray observations covered this area of the sky to help investigate the effects of the surrounding intercluster medium on the radio source.

¹ <https://skyserver.sdss.org/dr12/en/tools/chart/navi.aspx>

Table 2. Properties of the peculiar radio source.

Source name	J1615+5452
RA (J2000)	16h15m31.1s
DEC (J2000)	+54d52m28s
z	0.32936
S_{150}	81.1 ± 6.3 mJy
S_{325}	50.5 ± 2.5 mJy
S_{610}	24.8 ± 1.2 mJy
S_{1400}	6.7 ± 0.8 mJy
α_{150}^{1400}	-1.12 ± 0.06
α_{150}^{1400}	-1.58 ± 0.15
α_{610}^{610}	-1.12 ± 0.11
α_{325}^{325}	-0.61 ± 0.12
α_{150}^{150}	-0.97 ± 0.19
$\Delta\alpha$ (SCP)	-0.97 ± 0.19
$L_{1.4\text{GHz}}$	$2.64 \times 10^{24} \text{ W Hz}^{-1}$

**Figure 1.** The 610 MHz radio continuum contours (levels $-2, 2, 3, 5, 10, 30, 40, 45, 48, 50 \times \sigma$ ($40 \mu\text{Jy}/\text{beam}$)) overlaid on the SDSS-DR12 i -band image. The cross is the centroid of the radio emission. The filled ellipse in the lower left represents the FWHM contour of the synthesized beam at 610 MHz.

3.2 Morphology and flux densities

Figure 2 shows the radio images at all four frequencies. As noted in Table 1, the GMRT angular resolution ranges from 6 arcsec at 610 MHz to 20 arcsec at 150 MHz. We used PyBDSF (Mohan & Rafferty 2015) to measure the flux density of the source from all the available images. The derived values are presented in Table 2 with the associated errors σ_1 computed following the expression outlined by Hopkins et al. (2003) but with a slight modification to account for our instrumen-

tal and pointing errors:

$$\sigma_1 = I \sqrt{2.5 \left(\frac{\sigma}{I} \right)^2 + 0.05^2} \quad (1)$$

where I is the integrated flux density and σ the local rms noise.

We first noticed the peculiarity of J1615+5452 by cross-matching the GMRT 610 MHz radio image of EN1 with the high resolution 1.4 GHz VLA data. While the source is easily detectable at 610 MHz with a projected linear size of ~ 92 kpc (0.31 arcmin) at $z \sim 0.33$ and a flux density of $S_{610} = 24.8 \pm 1.2$ mJy, no 1.4 GHz contours however, have been recovered. The VLA high resolution images did not reveal any compact core, jets or hotspots. Such a non-standard morphological structure is worth an investigation as it was also observed by e.g. Brienza et al. (2016) when studying a remnant radio galaxy in a particularly low-density environment.

The radio emission is also featured at 150 MHz with a flux density of $S_{150} = 81.1 \pm 6.3$ mJy. In the 325 MHz image, the source has extended diffuse emission with $S_{325} = 50.5 \pm 2.5$ mJy and a projected linear size of 100 kpc (0.34 arcmin). The source extraction with PyBDSF in the low resolution NVSS data resulted in a flux density of $S_{1400} = 6.7 \pm 0.8$ mJy which translates to a radio luminosity of $L_{1.4\text{GHz}} = 2.64 \times 10^{24} \text{ W Hz}^{-1}$.

We also estimated an upper limit of the radio core prominence (CP) which is a parameter used by e.g. Giovannini et al. (1988), Hardcastle et al. (2016), Brienza et al. (2016, 2017), Mahatma et al. (2018) in their search for candidate remnant AGNs. This was done by taking the ratio between the 3σ local rms noise in the high resolution VLA image from Banfield et al. (2011) and the total flux density at 150 MHz. We derived a value of $\text{CP} \lesssim 3.3 \times 10^{-3}$. However, given that this value changes depending on the observing frequencies and that a low core prominence is expected for a flat-spectrum core component combined with a steep-spectrum of the total radio emission (Hardcastle & Looney 2008), we also considered an alternative method to investigate the AGN activity in the core. By taking the value of $L_{1.4\text{GHz}}$, we used the following empirical relation established by de Ruiter et al. (1990):

$$\log \text{CP} = -0.55 \log L_{1.4\text{GHz}} + 11.76 \quad (2)$$

to predict a much higher value of $\text{CP} \sim 0.02$. The de Ruiter et al. (1990) relation states that the CP is inversely proportional to the radio power, i.e. low luminosity radio sources (with radio powers smaller than $10^{26} \text{ W Hz}^{-1}$) are expected to have a relatively higher CP compared to the high luminosity ones.

The values of the core prominence and the absence of the compact radio structure suggest that J1615+5452 could be a dying AGN (see Section 5). The analysis of the source radio spectrum in Section 3.3 will help determine whether the AGN activity has indeed switched off.

3.3 Radio spectrum

In the active stage, a broken power-law fit also known as the CI model (Kardashev 1962; Jaffe & Perola 1973) best describes the radio source spectrum with a spectral index $\alpha \sim \alpha_{\text{inj}}$ below the break frequency and $\alpha < \alpha_{\text{inj}} - 0.5$ above

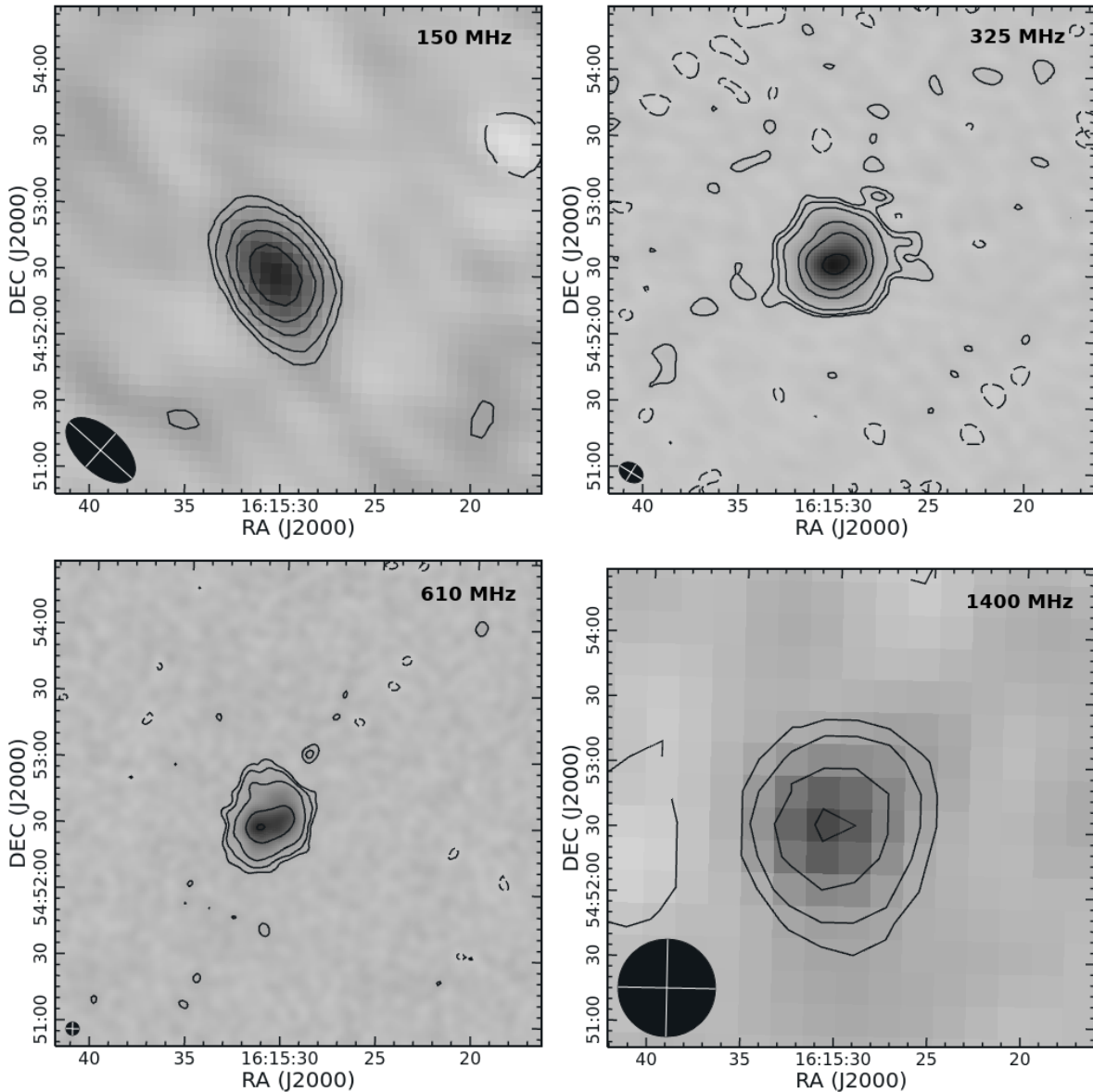


Figure 2. Radio maps of the source J1615+5452 with the synthesized beam shown in the bottom left corner. Overlaid are the total intensity contours: (*top left*) GMRT 150 MHz map, levels $-2, 2, 3, 5, 7, 10 \times \sigma$ (3.1 mJy/beam); (*top right*) GMRT 325 MHz map, levels $-3, 3, 5, 10, 30, 50, 100 \times \sigma$ ($70 \text{ } \mu\text{Jy/beam}$); (*bottom left*) GMRT 610 MHz map, levels $-3, 3, 5, 10, 30, 50 \times \sigma$ ($40 \text{ } \mu\text{Jy/beam}$); (*bottom right*) NVSS 1400 MHz map, levels $-2, 2, 3, 5, 7, \times \sigma$ (0.34 mJy/beam).

ν_b . If the source is young enough and the observing frequency range is limited to $\sim \text{GHz}$ frequencies, then a simple power-law with $\alpha \sim \alpha_{\text{inj}}$ produces a reasonable fit to its radio spectrum still unaffected by the radiative losses.

For J1615+5452, the best fit model² of the integrated spectrum (see Figure 3) is a broken power-law fit combined with an exponential break frequency $\nu_{b, \text{exp}}$. At low frequencies, the spectral shape is typical of active radio galaxies with an index of $\alpha_{150}^{325} = -0.61 \pm 0.12$. Steep spectra with $\alpha_{325}^{610} = -1.12 \pm 0.11$ and $\alpha_{610}^{1400} = -1.58 \pm 0.15$ are, however, recorded above a certain spectral break likely occurring be-

tween 325 and 610 MHz. The value of such a parameter and the resulting synchrotron age are derived in Section 4.2.

In the frequency range 150 - 1400 MHz, $\alpha_{150}^{1400} = -1.12 \pm 0.06$ and the spectral curvature parameter $\Delta\alpha = \alpha_{610}^{1400} - \alpha_{150}^{325}$ is equal to -0.97 ± 0.19 . The measured values of the SCP and the spectral indices are reported in Table 2.

The spectral break at low frequencies, the steep high frequency spectra as well as a SCP $\ll -0.5$ imply the predominance of nonthermal synchrotron emission and the central engine switch off. Such characteristic features of the spectra classify once again J1615+5452 as a dying radio AGN (e.g. Parma et al. 2007; Murgia et al. 2011; Brienza et al. 2016).

² The best fit Cl_{off} model by Komissarov & Gubanov (1994) is briefly described in Section 4.2.

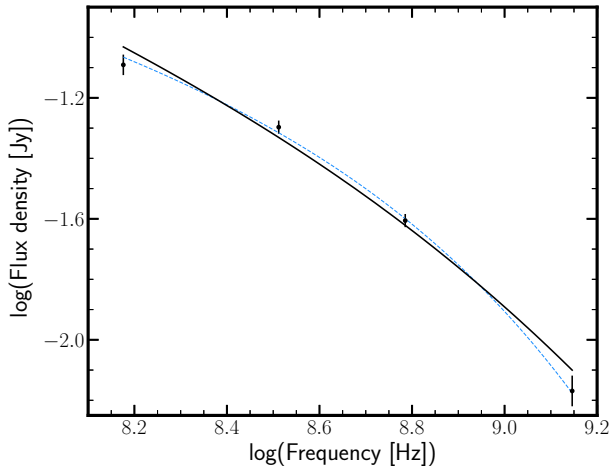


Figure 3. The integrated radio spectrum of the candidate remnant radio AGN J1615+5452. The dashed line represents the best fit CI_{off} model (though associated with a relatively flat injection index of 0.40). For $\alpha_{\text{inj}} = 0.61$ and $B_{\text{eq}} = 4.1 \mu\text{Jy}$, the same model returns the solid line with an observed break frequency $\nu_b \sim 384$ MHz and an off component break at 5 GHz.

4 INVESTIGATING THE DYING RADIO AGN

4.1 Source energetics

A first order approximation of the synchrotron age requires an estimate of the magnetic field strength. We assume minimum energy conditions between particles and magnetic field to derive the equipartition magnetic field B_{eq} which is given by

$$B_{\text{eq}}[\text{G}] = \left(\frac{24\pi}{7} u_{\text{min}} \right)^{1/2}. \quad (3)$$

Assuming an uniform magnetic field and an isotropic particle distribution, we computed the minimum energy density u_{min} following the Govoni & Feretti (2004) formula:

$$u_{\text{min}} \left[\frac{\text{erg}}{\text{cm}^3} \right] = \xi(\alpha, \nu_1, \nu_2)(1+k)^{4/7} (\nu_0 [\text{MHz}])^{-4\alpha/7} \\ \times (1+z)^{(12-4\alpha)/7} \left(I_0 \left[\frac{\text{mJy}}{\text{arcsec}^2} \right] \right)^{4/7} (d [\text{kpc}])^{-4/7} \quad (4)$$

where the parameter ξ is dependent on frequencies ($\nu_1 = 10$ MHz and $\nu_2 = 100$ GHz) and the synchrotron spectral index $\alpha < 0$ presumed for the observed spectrum; k is the relativistic proton-to-electron energy density ratio. I_0 is the source surface brightness measured at the frequency ν_0 and d is the source depth.

At $\alpha = -0.61$ with $\nu_0 = 325$ MHz, we find $u_{\text{min}} = 1.54 \times 10^{-12} \text{ erg cm}^{-3}$ and $B_{\text{eq}} \sim 4.1 \mu\text{G}$. The other parameters in Eq. 4 are as follows: $k = 1$, $I_0 = 0.43 \text{ mJy/arcsec}^2$, and $d \sim 100$ kpc (the average of the angular extents of the source). Note that the value of α is consistent with the observed injection index α_{inj} measured at ν_0 where the steepening is still not affecting the shape of the radio spectrum. Regarding the frequency interval, the choice of a relatively low value of $\nu_1 = 10$ MHz is motivated by the importance of the energy density of relativistic electrons radiating their energy at lower frequencies (e.g. Pacholczyk 1970; Beck &

Krause 2005). The value of ν_2 is however less critical for the minimum energy estimates. In fact, if $\nu_2 = 10$ GHz for $\alpha = -0.61$, u_{min} only decreases by 9 percent from its current value.

Previous works have reported that the classical formula used to calculate B_{eq} may underestimate the magnetic field strength because of inadequate assumptions of the frequency integration limits (e.g. Brunetti et al. 1997; Beck & Krause 2005). A revised estimate is:

$$B'_{\text{eq}} [\text{G}] \sim 1.1 \gamma_{\text{min}}^{\frac{1+2\alpha}{3-\alpha}} B_{\text{eq}}^{\frac{7}{2(3-\alpha)}} \quad (5)$$

where B'_{eq} is a modified equipartition magnetic field based on a limit of the Lorentz factors γ assuming $\gamma_{\text{max}} \gg \gamma_{\text{min}}$. For $\gamma_{\text{min}} = 100$ and $\gamma_{\text{max}} = 10^6$, we find $B'_{\text{eq}} \sim 4.9 \mu\text{G}$ using the 325 MHz radio emission. Because of the flat radio spectrum at low frequencies, we only expect $\sim 20 - 30$ percent deviation of the revised value from the classical B_{eq} (Beck & Krause 2005). In this work, such a variation is only around 16 percent. We thus adopt the magnetic field strength $B_{\text{eq}} \sim 4.1 \mu\text{G}$ in the remainder of this work.

4.2 Synchrotron age

With estimates of the magnetic field strength B_{eq} and the break frequency ν_b , one can calculate to first order the spectral age t_s using the following expression (Murgia et al. 2011):

$$t_s [\text{Myr}] = 1590 \left[\frac{(B_{\text{eq}} [\mu\text{G}])^{1/2}}{(B_{\text{eq}}^2 + (B_{\text{IC}} [\mu\text{G}])^2)(1+z)^{1/2} (\nu_b [\text{GHz}])^{1/2}} \right] \quad (6)$$

where $B_{\text{IC}} = 3.25(1+z)^2$ is the Inverse Compton equivalent magnetic field. By setting a lower limit to the break frequency such that $\nu_b = 610$ MHz, an upper limit to the source age is in the order of 120 Myr.

We also run BRATS³ (Harwood et al. 2013, 2015) to fit the radio spectrum and to ultimately get a more robust estimate of the synchrotron age. Given the remnant nature of the source, we fit the KGJP model to the data. This remnant radio emission model developed by Komissarov & Gubanov (1994) is also known as the CI_{off} model and it is a modification of the standard continuous injection model (Kardashev 1962; Jaffe & Perola 1973) to account for the AGN switch off.

By considering an injection index $\alpha_{\text{inj}} = -0.61$ (the spectral index at low frequencies), a minimum and maximum Lorentz factor of $\gamma_{\text{min}} = 100$ and $\gamma_{\text{max}} = 10^6$, a magnetic field strength $B_{\text{eq}} = 4.1 \mu\text{G}$, with the other input parameters set to their default values, BRATS returns a fitted age of $t_s = 76.0^{+7.4}_{-8.7}$ Myr, a break frequency $\nu_b = 384$ MHz and an off component break $\nu_{b, \text{exp}} = 5029$ MHz. The timescales during active ($t_{\text{on}} = 54.9^{+7.4}_{-8.5}$ Myr) and quiescent ($t_{\text{off}} = 21.0^{+0.0}_{-2.1}$ Myr) phases were also computed. With $t_s = t_{\text{on}} + t_{\text{off}}$, we get a t_{off}/t_s ratio of ~ 0.3 . The off component

³ The Broadband Radio Astronomy ToolS is a software package that uses spectral ageing models to derive the properties and morphology of a radio source. For more details, visit <http://www.askanastronomer.co.uk/brats>.

break frequency, $\nu_{b, \text{exp}} = \nu_b (t_s/t_{\text{off}})^2$, does not lie within the available frequency coverage because the source is observed soon after the radio core switch off according to the fitting model, i.e. the timescale of the quiescence phase is significantly shorter than that of the active phase (Parma et al. 2007). In that case, $\Delta\alpha \sim -1$ (derived in Section 3.3) can only be considered as an upper limit of the spectral curvature parameter.

The source age of 76 Myr is in agreement with the source morphology and the steep spectral properties reported in Section 3. Note, however, that the computed value is dependent on some critical parameters such as α_{inj} . For instance, the derived age falls between 37 - 106 Myr while varying the injection index α_{inj} between 0.5 and 0.8. Such a range is consistent with the upper limit to the source age as well as the typical ages (a few tens of Myr) for dying radio galaxies (e.g. Blandford & Ostriker 1978; Murgia et al. 2011; Brienza et al. 2016).

Although we can achieve the best fit model with $\alpha_{\text{inj}} = 0.40$ and $B_{\text{eq}} = 12.5 \mu\text{G}$ as free parameters ($\chi_{\text{red}}^2 = 1.42$, dashed line in Figure 3), we decided to consider BRATS outputs associated with fixed values of $\alpha_{\text{inj}} = 0.61$ and $B_{\text{eq}} = 4.1 \mu\text{G}$. The latter parameters are consistent with the radio properties of the source (e.g. the spectral index at lower frequencies) and the resulting model still gives a reasonable fit to the radio spectrum ($\chi_{\text{red}}^2 = 8.86$, solid line in Figure 3). Table 3 summarizes BRATS fitting results in both cases.

5 DISCUSSION

A low core prominence may result from the very weak or no core emission, a potential evidence of the central AGN switch off. In the case of J1615+5452, the observed core prominence of $\lesssim 3.3 \times 10^{-3}$ falls within the range of CP $< 10^{-4} - 5 \times 10^{-3}$ that are associated with the remnant radio sources from the literature (e.g. Giovannini et al. 1988; Hardcastle et al. 2016; Brienza et al. 2017; Mahatma et al. 2018). Such a low value is well below CP ~ 0.02 (the CP value expected for a source of the same radio power assuming the empirical correlation found by de Ruiter et al. 1990) and it is in agreement with a quiescent nuclear engine or an active one but at a very weak level than what is observed in typical radio sources. Furthermore, the value of CP ~ 0.02 also falls within the interval of 0.1 - 0.001, which is a CP range reported by de Ruiter et al. (1990) for B2 sources with radio powers between $10^{24} - 10^{26} \text{WHz}^{-1}$ including a very small fraction of remnant radio AGNs. Nevertheless, classifying a radio source as a remnant based only on its core activity is deemed unreliable, especially for lower resolution and sensitivity observations where a faint core may be missed (e.g. Mahatma et al. 2018). It is thus recommended to combine this parameter with other selection criteria to achieve unbiased detection (e.g. Brienza et al. 2017).

In this work, $\alpha_{325}^{1400} = -1.37 \pm 0.09$ and $\Delta\alpha \sim -0.97 \pm 0.19$. These spectral characteristics are comparable to those of the complete samples of remnant radio galaxies drawn by Parma et al. (2007) and Murgia et al. (2011). The former authors define a dying radio source based on steep spectral shape ($\alpha_{325}^{1400} < -1.3$) and the absence of compact radio structures, whereas the latter consider as well the source spectral cur-

Table 3. Fitting results from BRATS Cl_{off} model.

α_{inj}	B_{eq} [μG]	ν_b [MHz]	$\nu_{b, \text{exp}}$ [MHz]	t_s [Myr]	t_{off}/t_s	χ_{red}^2
(1)	(2)	(3)	(4)	(5)	(6)	(7)
0.40	12.5	347	1024	$35.9^{+1.9}_{-3.5}$	0.6	1.42
0.61	4.1	384	5029	$76.0^{+7.4}_{-8.7}$	0.3	8.86

Notes. Columns 1 & 2: the injection index and the magnetic field as input parameters; Column 3: the break frequency; Column 4: the off-component break frequency; Columns 5 & 6: the computed synchrotron age of the source and the ratio between the quiescent and the active timescales; Column 7: the reduced chi-square of the fit.

vature ($\Delta\alpha < -0.5$) as one of its complementary selection criteria to search for candidate remnant AGNs.

In addition, J1615+5452 has similar spectral properties with those of remnant radio galaxies observed in the LOFAR Lockman Hole field ($\alpha_{150}^{1400} < -1.2$ and $\Delta\alpha = \alpha_{325}^{1400} - \alpha_{150}^{325} < -0.5$, Brienza et al. 2017). Note however that the source spectral index $\alpha_{125}^{325} = -0.61 \pm 0.12$ at low frequencies is consistent with the spectra of active radio galaxies. Murgia et al. (2011) and Brienza et al. (2016) also noticed such spectral shape while investigating the radio properties of B2 1619+29 and blob1 (a remnant radio galaxy in the LOFAR field), respectively. A slow rate of radiative cooling or a young plasma are suggested to explain the observed spectral feature. It is therefore crucial to carry multi-frequency analyses for an optimal detection of genuine dying radio sources with such spectra.

The computed magnetic field $B_{\text{eq}} = 4.1 \mu\text{G}$ is in agreement with the magnetic field strengths of previously studied remnant radio AGNs (e.g. Murgia et al. 2011; de Gasperin et al. 2014; Brienza et al. 2016; Duchesne & Johnston-Hollitt 2019) and dying giant radio galaxies (e.g. Tamhane et al. 2015) of the order of a few μG . Such a weak magnitude implies the predominance of the Inverse Compton scattering from the CMB over the synchrotron losses throughout the radiative cooling of the diffuse plasma (Komissarov & Gubanov 1994).

The age range of the source in Section 4.2 is comparable to those of other dying AGNs such as B2 0924+30 (54 Myr by Jamroz et al. 2004, ~ 88 Myr by Shulevski et al. 2017, 78 Myr by Turner 2018), the median age of the remnant samples from the Westerbork Northern Sky Survey (63 Myr, Parma et al. 2007) and blob1 (75 Myr, Brienza et al. 2016). With $t_s = 76$ Myr, the source is relatively older than the low luminosity radio galaxies from the B2 sample with a median age of 31 Myr (Parma et al. 1999).

By spending 30 percent of its lifetime in the quiescent phase, the t_{off}/t_s ratio of J1615+5452 fits within the range 0.2 - 0.8 reported in Parma et al. (2007) and Murgia et al. (2011). Once the dormant phase of the nuclear engine kicks off, either permanently or intermittently, the source compact radio structure will (partially) disappear due to the lack of freshly injected particles.

The diffuse radio emission of the source at low frequencies is similar to the peculiar morphology of other dying radio AGNs such as B2 0924+30 and blob1 which were also discovered (partly) because of their amorphous radio emission. Assuming that the host galaxy resides in a loose group

environment (see Section 3.1), then J1615+5452 also resembles to these two sources in a way that they are among the few known examples of non cluster-based dying radio galaxies (Jamrozy et al. 2004; de Gasperin et al. 2014; Hurley-Walker et al. 2015; Duchesne & Johnston-Hollitt 2019).

Finally, based on the different stages of the core activity (assuming the AGN lifecycle is tightly related to the accretion of matter onto the SMBH), the population of radio galaxies can be classified into three broad categories: the active, the dying and the restarted ones (Cordey 1987; Morganti 2017). In the case of an intermittently active radio source, the nuclear engine undergoes multiple cycles of AGN activity of the order of $\sim 10^5$ yr instead of a continuous activity with a single accretion phase that usually lasts $10^7 - 10^9$ yr (Marconi et al. 2004; Schawinski et al. 2015). During the quiescent AGN phase, the nuclear activity is either significantly reduced or temporarily switched off due to a shortage of material accreting onto the SMBH. The central engine of the nuclear activity will eventually reignite once a new phase of accretion onto the SMBH starts again. Such a rejuvenation of AGN activity is deemed responsible for the presence of a flat-spectrum radio core that co-exists with remnant radio lobes from past nuclear activity (e.g. Saikia & Jamrozy 2009; Morganti 2017). With no direct evidence of a restarted core and/or new born jets for the current source, and based on the derived characteristics in Sections 3 and 4, we potentially classify J1615+5452 as a dying radio AGN. This implies that the radio core no longer fuels fresh particle injection. The fossil radio lobes, however, remain visible (up to $\sim 10^8$ yr depending on the radio source environment) because of the radiating low energy particles being relatively unaffected by the fast spectral evolution.

6 SUMMARY AND CONCLUSIONS

We have presented in this paper the discovery of a candidate remnant radio galaxy J1615+5452 in the ELAIS-N1 field. Using low frequency GMRT observations combined with archival VLA data, we derived the source flux densities between 150 and 1400 MHz to investigate the source radio spectrum. Our main results are summarized below:

(i) The candidate remnant AGN is likely associated with an early-type elliptical galaxy at redshift of $z \sim 0.33$. The potential host galaxy appears to reside in a low-density environment.

(ii) With an angular extent of ~ 100 kpc, J1615+5452 has a diffuse amorphous radio emission with no evidence of compact core, jets and hotspots. We also did not detect radio counterparts in the 1.4 GHz VLA data with a high resolution of ~ 5 arcsec.

(iii) The spectral indices between 150 and 1400 MHz vary between -0.6 and -1.6 which give a high spectral curvature $\Delta\alpha \sim -1$. Such spectral features indicate the predominance of nonthermal synchrotron emission with strong ongoing radiative losses.

(iv) The radio spectrum is reasonably described by a CI_{off} model with a break frequency $\nu_b = 384$ MHz and an off component break at $\nu_{b, \text{exp}} \sim 5$ GHz. The computed synchrotron age is $t_s = 76.0^{+7.4}_{-8.7}$ Myr with $t_{\text{on}} = 54.9^{+7.4}_{-8.5}$ Myr

and $t_{\text{off}} = 21.0^{+0.0}_{-2.1}$ Myr. The source is estimated to have spent 30 percent of its total lifetime in the fading phase.

The morphological characteristics of J1615+5452 coupled with its spectral properties and synchrotron age helped us to classify the peculiar source as a dying radio galaxy. Combining such analyses is key to identify elusive remnant radio AGNs that play an important role toward a comprehensive understanding of AGN evolution in general. With new or upgraded low frequency radio interferometers such as LOFAR and the upgraded GMRT (uGMRT, Gupta et al. 2017), ongoing analyses of deep radio surveys are expected to significantly increase the detection of these rare sources. Furthermore, prior the completion of the Square Kilometre Array⁴ (SKA), instruments like the Australian SKA Pathfinder (ASKAP, Johnston et al. 2008) and the South African MeerKAT telescope (Jonas & MeerKAT Team 2016; Camilo et al. 2018) are also expected to provide GHz frequency observations with arcsec resolution and unprecedented sensitivities to large scale structures. Such capabilities are ideal for identifying remnant radio galaxies despite the source spectral evolution.

ACKNOWLEDGEMENTS

The authors thank the referee for detailed comments and constructive suggestions. We are also grateful to the staff of the GMRT that made these observations possible. GMRT is run by the National Centre for Radio Astrophysics of the Tata Institute of Fundamental Research. This work has made use of the Cube Analysis and Rendering Tool for Astronomy (CARTA, Comrie et al. 2018). ZR acknowledges the support and funding from the South African Astronomical Observatory and the South African Radio Astronomy Observatory, which are facilities of the National Research Foundation, an agency of the Department of Science and Innovation. CHIC acknowledges the support of the Department of Atomic Energy, Government of India, under the project 12-R&D-TFR-5.02-0700.

DATA AVAILABILITY

The data underlying this article are available in Table 2 of the article. This publication makes use of archival GMRT datasets and VLA image available at <https://naps.ncra.tifr.res.in/goa/> and <https://www.cv.nrao.edu/nvss/>, respectively. GMRT radio images will be shared on reasonable request to the corresponding author.

REFERENCES

- Abolfathi B., et al., 2018, ApJS, 235, 42
 Alam S., et al., 2015, ApJS, 219, 12
 Banfield J. K., George S. J., Taylor A. R., Stil J. M., Kothes R., Scott D., 2011, ApJ, 733, 69
 Beck R., Krause M., 2005, Astronomische Nachrichten, 326, 414
 Becker R. H., White R. L., Helfand D. J., 1995, ApJ, 450, 559

⁴ <https://www.skatelescope.org>

- Blandford R. D., Ostriker J. P., 1978, *ApJ*, 221, L29
- Brienza M., et al., 2016, *A&A*, 585, A29
- Brienza M., et al., 2017, *A&A*, 606, A98
- Brunetti G., Setti G., Comastri A., 1997, *A&A*, 325, 898
- Camilo F., et al., 2018, *ApJ*, 856, 180
- Chakraborty A., et al., 2019, *MNRAS*, 490, 243
- Cohen A. S., Lane W. M., Cotton W. D., Kassim N. E., Lazio T. J. W., Perley R. A., Condon J. J., Erickson W. C., 2007, *AJ*, 134, 1245
- Comrie A., et al., 2018, CARTA: The Cube Analysis and Rendering Tool for Astronomy, doi:10.5281/zenodo.3377984, <https://doi.org/10.5281/zenodo.3377984>
- Condon J. J., Cotton W. D., Greisen E. W., Yin Q. F., Perley R. A., Taylor G. B., Broderick J. J., 1998, *AJ*, 115, 1693
- Cordey R. A., 1986, *MNRAS*, 219, 575
- Cordey R. A., 1987, *MNRAS*, 227, 695
- Duchesne S. W., Johnston-Hollitt M., 2019, *PASA*, 36, e016
- Fabian A. C., 2012, *ARA&A*, 50, 455
- Garn T., Green D. A., Riley J. M., Alexander P., 2008, *MNRAS*, 383, 75
- Gentile G., Rodríguez C., Taylor G. B., Giovannini G., Allen S. W., Lane W. M., Kassim N. E., 2007, *ApJ*, 659, 225
- Giovannini G., Feretti L., Gregorini L., Parma P., 1988, *A&A*, 199, 73
- Govoni F., Feretti L., 2004, *International Journal of Modern Physics D*, 13, 1549
- Grant J. K., Taylor A. R., Stil J. M., Landecker T. L., Kothes R., Ransom R. R., Scott D., 2010, *ApJ*, 714, 1689
- Gupta Y., et al., 2017, *Current Science*, 113, 707
- Hardcastle M. J., Looney L. W., 2008, *MNRAS*, 388, 176
- Hardcastle M. J., et al., 2016, *MNRAS*, 462, 1910
- Harwood J. J., Hardcastle M. J., Croston J. H., Goodger J. L., 2013, *MNRAS*, 435, 3353
- Harwood J. J., Hardcastle M. J., Croston J. H., 2015, *MNRAS*, 454, 3403
- Hopkins A. M., Afonso J., Chan B., Cram L. E., Georgakakis A., Mobasher B., 2003, *AJ*, 125, 465
- Hurley-Walker N., et al., 2015, *MNRAS*, 447, 2468
- Intema H. T., van der Tol S., Cotton W. D., Cohen A. S., van Bemmel I. M., Röttgering H. J. A., 2009, *A&A*, 501, 1185
- Intema H. T., Jagannathan P., Mooley K. P., Frail D. A., 2017, *A&A*, 598, A78
- Jaffe W. J., Perola G. C., 1973, *A&A*, 26, 423
- Jahnke K., Macciò A. V., 2011, *ApJ*, 734, 92
- Jamrozy M., Klein U., Mack K.-H., Gregorini L., Parma P., 2004, *A&A*, 427, 79
- Jelić V., et al., 2014, *A&A*, 568, A101
- Johnston S., et al., 2008, *Exp. Astron.*, 22, 151
- Jonas J., MeerKAT Team 2016, in *MeerKAT Science: On the Pathway to the SKA*. p. 1
- Jurlin N., et al., 2020, arXiv e-prints, p. arXiv:2004.09118
- Kapińska A. D., Uttley P., Kaiser C. R., 2010, *Birth and Evolution of Radio Galaxies*. p. 337
- Kardashev N. S., 1962, *Soviet Ast.*, 6, 317
- Kennicutt Jr. R. C., 1992, *ApJS*, 79, 255
- Komissarov S. S., Gubanov A. G., 1994, *A&A*, 285, 27
- Konar C., Hardcastle M. J., Jamrozy M., Croston J. H., 2013, *MNRAS*, 430, 2137
- Kormendy J., Ho L. C., 2013, *ARA&A*, 51, 511
- Lonsdale C. J., et al., 2009, *IEEE Proceedings*, 97, 1497
- Mahatma V. H., et al., 2018, *MNRAS*, 475, 4557
- Marconi A., Risaliti G., Gilli R., Hunt L. K., Maiolino R., Salvati M., 2004, *MNRAS*, 351, 169
- Mohan N., Rafferty D., 2015, *PyBDSF: Python Blob Detection and Source Finder*, *Astrophysics Source Code Library* (ascl:1502.007)
- Morganti R., 2017, *Nature Astronomy*, 1, 596
- Murgia M., et al., 2011, *A&A*, 526, A148
- Ocran E. F., Taylor A. R., Vaccari M., Ishwara-Chandra C. H., Prandoni I., 2020, *MNRAS*, 491, 1127
- Oliver S., et al., 2000, *MNRAS*, 316, 749
- Pacholczyk A. G., 1970, *Radio astrophysics. Nonthermal processes in galactic and extragalactic sources*. San Francisco, Freeman
- Parma P., Murgia M., Morganti R., Capetti A., de Ruiter H. R., Fanti R., 1999, *A&A*, 344, 7
- Parma P., Murgia M., de Ruiter H. R., Fanti R., Mack K.-H., Govoni F., 2007, *A&A*, 470, 875
- Planck Collaboration et al., 2016, *A&A*, 594, A13
- Saikia D. J., Jamrozy M., 2009, *Bulletin of the Astronomical Society of India*, 37
- Saripalli L., Subrahmanyan R., Thorat K., Ekers R. D., Hunstead R. W., Johnston H. M., Sadler E. M., 2012, *ApJS*, 199, 27
- Schawinski K., Koss M., Berney S., Sartori L. F., 2015, *MNRAS*, 451, 2517
- Shabala S. S., Jurlin N., Morganti R., Brienza M., Hardcastle M. J., Godfrey L. E. H., Krause M. G. H., Turner R. J., 2020, *MNRAS*,
- Shulevski A., Morganti R., Oosterloo T., Struve C., 2012, *A&A*, 545, A91
- Shulevski A., et al., 2017, *A&A*, 600, A65
- Sijacki D., Vogelsberger M., Genel S., Springel V., Torrey P., Snyder G. F., Nelson D., Hernquist L., 2015, *MNRAS*, 452, 575
- Silk J., Rees M. J., 1998, *A&A*, 331, L1
- Sirothia S. K., Dennefeld M., Saikia D. J., Dole H., Riquebourg F., Roland J., 2009, *MNRAS*, 395, 269
- Slee O. B., Roy A. L., Murgia M., Andernach H., Ehle M., 2001, *AJ*, 122, 1172
- Sohn B. W., Klein U., Mack K.-H., 2003, *A&A*, 404, 133
- Swarup G., 1991, *Proceedings of the IAU Colloquium 131: Radio interferometry. Theory, techniques, and applications*, eds. T. J. Cornwell & R. A. Perley, 19, 376
- Tamhane P., Wadadekar Y., Basu A., Singh V., Ishwara-Chandra C. H., Beelen A., Sirothia S., 2015, *MNRAS*, 453, 2438
- Taylor A. R., Jagannathan P., 2016, *MNRAS*, 459, L36
- Tingay S. J., et al., 2013, *PASA*, 30, 7
- Turner R. J., 2018, *MNRAS*, 476, 2522
- de Gasperin F., Intema H. T., Williams W., Brügger M., Murgia M., Beck R., Bonafede A., 2014, *MNRAS*, 440, 1542
- de Ruiter H. R., Parma P., Fanti C., Fanti R., 1990, *A&A*, 227, 351
- van Haarlem M. P., et al., 2013, *A&A*, 556, A2

This paper has been typeset from a $\text{\TeX}/\text{\LaTeX}$ file prepared by the author.